Preprints.org

Article

Using SPS Sintering System in Fabrication of Advanced Semiconductor Materials

Kamil Kaszyca [*] , Marcin Chmielewski , Bartosz Bucholc , Piotr Błyskun , Fatima Nisar , Jerzy Rojek , Rafał Zybała

Article

Using SPS Sintering System in Fabrication of Advanced Semiconductor Materials

Kamil Kaszyca [1] , **Marcin Chmielewski** [1] , **Bartosz Bucholc** [1,2] , **Piotr Błyskun** [3] , **Fatima Nisar** [2] , **Jerzy Rojek** [2] **and Rafał Zybała** [1,3]

[1]   Lukasiewicz Research Network, Institute of Microelectronics and Photonics, al. Lotnikow 32/46, 02-668 Warsaw, Poland

[2]   Institute of Fundamental Technological Research, Polish Academy of Sciences, Pawinskiego 5B, 02-106 Warsaw, Poland

[3]   Faculty of Materials Science and Engineering, Warsaw University of Technology, Woloska 141, 02-507 Warsaw, Poland

*   Correspondence: Kamil.Kaszyca@imif.lukasiewicz.gov.pl

Abstract: The interest in the Spark Plasma Sintering (SPS) technique has continuously increased over the last few years. This article shows the possibility of the development of a SPS device used for material processing and synthesis both in both scientific and industrial applications. This work presents an example of processing Arc-Meleted (half-Heusler, cobalt triantimonide) and SHS-synthesized semiconductors (bismuth telluride) materials with SPS device. The system functionalities expansion is presented, showing the possible way of increasing the information amount obtained about SPS processes and using the SPS apparatus for conducting synthesis of materials and increasing reproducibility and accuracy of process parameters control.

Keywords: spark plasma sintering; arc melting; semiconductor materials; half-Heusler; bismuth telluride; cobalt triantimonide; SHS; SPS

---

1. Introduction

Currently Materials Engineers are mostly focused on the development of new materials, characterized by higher operational parameters, but this forces also the development of materials fabrication methods, allowing to overcome the boundaries of conventional fabrication methods.

The increasing popularity of the SPS method [1] and its increased accessibility is visible in many publications that use SPS as the main method for materials forming and densification. The ability of fast heating and cooling enables the possibility of fabricating novel materials. The SPS technique allows to obtain a compact from powder in one production cycle. This enables the synthesis and formation of elements from materials sensitive to the influence of the external environment, for example, advanced semiconductor materials. Due to short sintering times, materials fabricated in Spark Plasma Sintering processes show much less grain growth and less probability of material decomposition.

The diagram of the SPS sintering equipment is shown in Figure 1. Processed material(3) is placed in a graphite die (1) and closed by two graphite punches (2). Then the die and the powder are placed between the device's electrodes in the vacuum chamber (5).
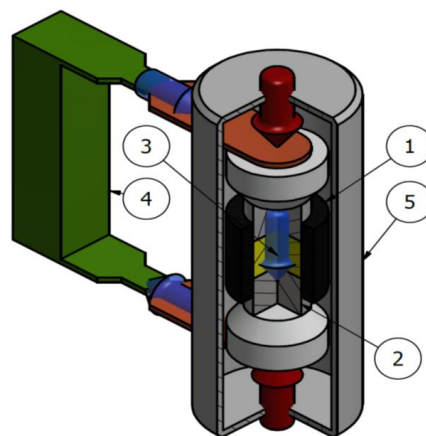
**Figure 1.** Scheme of the system for spark sintering using the SPS technique, 1 - die, 2 - punch, 3 - sintered material, 4 - power supply, 5 - vacuum chamber.

The current flowing through the matrix and powder causes the release of a large amount of Joule heat, heating the entire system. In some cases, during SPS sintering, arcing may occur between the sintered particles.

Figure 2 presents the diagram of the SPS model described in [2]. The presented model takes into account the geometry of the sintering elements and mentions basic process parameters, but simplifies the issue to a simple temperature/voltage/displacement functions output. The more advanced approach is presented in work [3], where the Authors compare grain growth as a function of temperature in transparent ceramics. Work [4] presents the comparison of simulated and experimental data of SPS sintered samples and applies the temperature-gradient issue to the created model. Cited works show the increase of complexity of research connected with modelling and justify the apparatus functionality expansion.
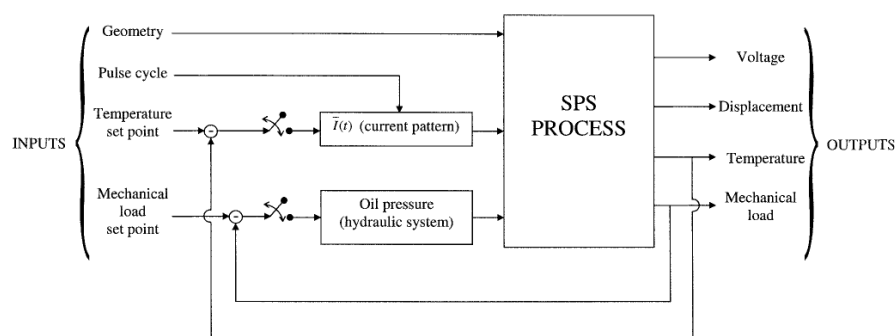
Figure 2. Idea of SPS process model described by Cincotti [2]

The basic, minimal set of information (process parameters) describing the SPS densification process is the following:

1. annealing temperature - the highest maintained temperature over a process
2. pressure - uniaxial pressure applied to the sample during the sintering process
3. time of highest temperature hold step.

Presented parameters are sufficient in most cases [5,6], but the development of mathematical models of the sintering process, novel techniques and materials need to be supported by a detailed description of sintering process parameters over time. This article shows the possibility of the development of a SPS device and the application of this device for semiconductor materials processing or synthesis in both scientific and industrial applications. The versatility and captivity of the SPS

technique make it a preferred solution solution for many different materials including biomaterials, nanomaterials and semiconductors.

The thermoelectric phenomenon allows direct conversion of heat into electrical energy. It occurs in almost all materials, but only a small group of semiconductors exhibit properties allowing for their practical usage for energy generation. Their conversion usefulness is parameterized by a *figure-of-merit* factor [7] (ZT) as defined in Equation (1).

$$ZT = \frac{\alpha^2 \times \sigma}{\kappa} \tag{1}$$

A good thermoelectric material exhibits high Seebeck coefficient (α), high electrical conductivity (σ) and low heat conductivity (κ). Such a combination of properties is rare and advanced fabrication methods have to be used to achieve it. There are two widely used mechanisms of ZT factor optimization: (1) doping the material can improve Seebeck coefficient and (2) electrical conductivity by introducing dopants to fabricate extrinsic semiconductors [8] and material structurization, having the most impact on thermal conductivity of material [9]. The reduction of heat conductivity can also occur if the dopant atoms significantly differ from the main semiconductor structure (eg. there is a significant difference in atomic masses) - this leads to phenomenon called phonon scattering [10,11] and it is a promising effect allowing reduction of lattice part of heat conductivity.

The first part of this work aims to show the possibilities of extension of the Spark Plasma Sintering apparatus and present example materials we have processed using our device. The most popular methods of synthesis of thermoelectric materials are direct synthesis of melted substrates [6,12,13] and mechanical alloying [12,14]. Despite the high popularity of mentioned methods, there is a possibility of the development of new methods allowing quick materials fabrication or enabling the synthesis of new, difficult-to-synthesize materials. This work presents two alternative methods of materials synthesis.

The second part of the presented work focuses on researching a method dedicated to the faster and less expensive synthesis technique called Self-propagating high-temperature synthesis (*SHS*), and we have used this method for magnesium silicide synthesis [15]. Although synthesis of Bi_2Te_3 based materials was discussed in works [16,17] the potential of use *SPS* apparatus gives researchers a ready-to-use tool, providing heating and protective atmosphere functionalities. Using the *SHS* method can reduce the synthesis time from about 30 to about 6 hours and does not require additional processing, such as sealing reagents inside a vacuum quartz tube.

Arc-melting (*AM*) was widely used in the metallurgical industry from 1970 [18] but, due to the increase of availability of laboratory-size units, this method also gained popularity over last few years in materials science [19], with success in fabrication of high entropy alloys [20–22].

The first presented example of use of SPS apparatus is the processing of arc-melted semiconductor half-Heusler material $Hf_{0.6}Zr_{0.4}NiSn_{1-x}Sb_x$ and the hafnium doped cobalt triantimonide semiconductor $Hf_xCo_4Sb_{11.5}Te_{0.5}$. The second presented example is the use of SPS apparatus for (*SHS*), which allows quick synthesis of semiconductor material in a one-step exothermic reaction. The main advantages of the SHS method are processing time reduction and the possibility of process scale-up. The *SHS* synthesis method is widely used for SiC synthesis [23,24]. The increasing popularity of *SHS* method is connected with its multiple adaptations for example in the cases of synthesis of bio-materials [25] and semiconductors [26].

The third part of this work presents the possibility of Spark Plasma Sintering apparatus extensions and examples of materials processed with this method. Most of work presented in publications focuses mostly on the synthesis/sintering parameters and the materials properties characterization. It also presents example of out-of-the-box application of system to provide a tool that simplifies the SHS reaction initiation and monitoring.

2. Materials and Methods

2.1. Materials

The following materials were fabricated or processed using the SPS technique. Additional details can be found in Table 1.

1. Arc-Melted semiconductor materials, *HCST-x* ($Hf_xCo_4Sb_{11.5}Te_{0.5}$) for x=[0, 0.01, 0.02, 0.05, 0.10] and *HZNSS-x* ($Hf_{0.6}Zr_{0.4}NiSn_{1-x}Sb_x$ for x=[0.01, 0.02, 0.05])
2. Bismuth-telluride based materials synthesized by SHS technique mateirals (PBSTS-xxs). The reference material (PBSTq), fabricated inside quartz vacuum tube is also included for comparison of properties of SHS serie.

Table 1. List of fabricated materials

Identification	Chemical formula	Processing method
HCST-01	$Hf_{0.01}Co_4Sb_{11.5}Te_{0.5}$	AM, SPS
HCST-02	$Hf_{0.02}Co_4Sb_{11.5}Te_{0.5}$	AM, SPS
HCST-05	$Hf_{0.05}Co_4Sb_{11.5}Te_{0.5}$	AM, SPS
HCST-10	$Hf_{0.10}Co_4Sb_{11.5}Te_{0.5}$	AM, SPS
HZNZZ-01	$Hf_{0.6}Zr_{0.4}NiSn_{0.99}Sb_{0.01}$	AM, SPS
HZNZZ-02	$Hf_{0.6}Zr_{0.4}NiSn_{0.98}Sb_{0.02}$	AM, SPS
HZNZZ-05	$Hf_{0.6}Zr_{0.4}NiSn_{0.95}Sb_{0.05}$	AM, SPS
PBSTq (pREF)	$Bi_{0.5}Sb_{1.5}Te_3$	Melting, SPS
PBSTS-01s	$Bi_{0.5}Sb_{1.5}Te_{2.9}Se_{0.1}$	SHS, SPS
PBSTS-06s	$Bi_{0.5}Sb_{1.5}Te_{2.4}Se_{0.6}$	SHS, SPS
PBSTS-12s	$Bi_{0.5}Sb_{1.5}Te_{1.8}Se_{1.2}$	SHS, SPS
PBSTS-18s	$Bi_{0.5}Sb_{1.5}Te_{1.2}Se_{1.8}$	SHS, SPS

2.2. SPS system

The device used in this work was constructed by the researchers of Łukasiewicz Research Network - Institute of Microelectronics and Photonics and is still maintained and developed by its creators. The operational parameters of the presented equipment are listed in Table 2.

Table 2. Presented apparatus operational parameters.

Parameter	Value/Range	unit
Operating temperature	RT-2000	°C
Sample diameter	10-50[1]	mm
Power supply max. current	5000	A
Power supply max. voltage	10	V
Ultimate vacuum	10^{-5}	mBar
Pressing force (max)	10	Tons

[1] Samples with higher diameters can be processed, however under lower pressures.

2.3. Arc Melting of half-Heusler and cobalt triantimonide

The Arc-Melting method was used to fabricate the alloys containing the elements with high differences in melting points. Using *AM* method allows to alloy or synthesize elements with a significant difference in melting points, for example, Hafnium (melting point at 2227°C) and Cobalt (1495°C). The substrates (in the form of a few pieces of substrate chips) were placed inside a copper reactor and melted in a protective *Ar* atmosphere. During the melting process, the heat energy was delivered to the substrates by an electrical arc. The heating process was repeated 3 to 5 times to remelt the material to ensure material homogeneity. The main parameters controlling the process are heating current, melting time and cycle count. In this research, a TIG welder with a current range up to 200*A*

was used as a power source. The obtained materials were further powdered and SPS sintered to a form of 10 diameter, 12mm height samples:

1. cobalt triantimonide: T=650°C, P=50MPa, time=15min
2. half-Heusler: T=1000°C, P=50MPa, time=25min.

2.4. Thermal and electrical parameters characterization

Thermal conductivity was measured using the LFA 457 apparatus (Netzch) [27]. The measurement was performed on a 10mm diameter 1 mm height disc in the inert Ar protective atmosphere in the temperature range RT-700K.

The measurement of the electrical properties of the material was performed by the SeebTest device, using the 4-wire method, according to the concept presented in Figure 3.
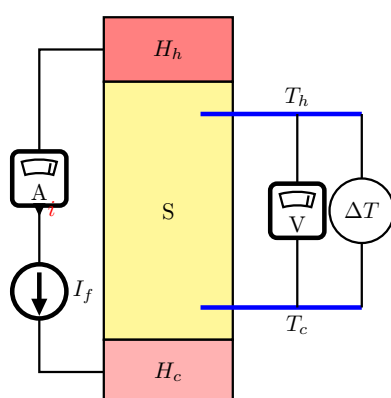
Figure 3. Scheme of the method implemented in the SeebTest device and a photo of the holder with the sample in the device, S - sample, H_h, H_c - upper/lower heater.

The measurement is performed on cylindrical samples with a 10 mm diameter and a height ranging from 10 to 14 mm. Electrodes T_h and T_c, placed in previously made holes with a precisely defined distance L_x, allow for simultaneous measurement of the voltage drop on the sample. The measurement takes place within a defined temperature range. The heating elements H_h, H_c stabilize the sample temperature. If the temperature of sample is stable the voltage drop on the sample is measured as a result of the alternating change in the direction of the predefined current flow. The heating elements then force a temperature gradient ΔT to determine the Seebeck coefficient α.

2.5. XRD diffraction

Phase composition studies using the X-ray diffraction technique were carried out using a Brucker D8 Advance device equipped with a Cu lamp. Measurements were done in the range from 10° to 120° (0.025° step), with a counting time of 3 seconds.

2.6. SHS Synthesis

SHS synthesis was conducted inside a graphite reactor placed in the SPS apparatus. The stoichiometric amounts of elements were homogenized using agate mortar and heated up to 500°C in an inert gas (Ar) atmosphere. Figure 4 shows the detailed heating program of the SHS reaction. There is a visible voltage drop at $Time = 250sec$, implied by the exothermic reaction. The process consists of two stages realized in one process:

1. Heating the reactor to 375°C and maintaining this temperature for 60 seconds. This step realizes the first, exothermic stage of materials synthesis (SHS occurs during the first initial heating)

2. Heating material to 475°C and maintaining this temperature for 300 seconds. This step was applied to fully react reagents and homogenize material
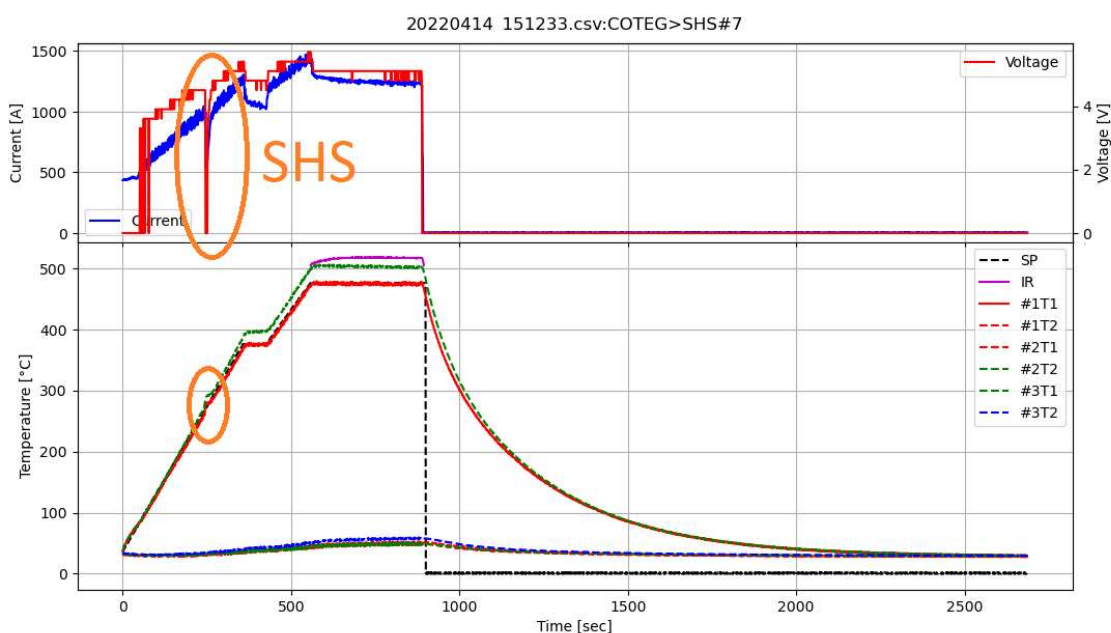

Figure 4. Full temperatures and power supply parameters over the SHS process in SPS apparatus. Voltage, Current - power supply readings, SP - Temperature Set Point, IR - Pyrometer temperature, #T - Temperatures (thermocouples)

The analysis of example process progress allows the determination of exothermic reaction occurrence by observing a significant drop of power delivered to the device. The samples after synthesis were powdered and sintered (450°C, 50MPa, 15 min) to 10 mm diameter samples and characterized.

2.7. Process data collection and device upgrade

SPS system upgrade idea model, presented in the Figure 5 is aimed to extend the control of process parameters during sintering and monitor their values over time. Figure 6 shows the collected parameters before(a) and after(b) device upgrade. The following changes were introduced:

1. Acquisition of power supply parameters (voltage and current), allowed to gain information about delivered power and, in some cases, the resistance of the sintering system.
2. Constant stabilization of pressing force. A hysteresis regulator was used previously, causing lower reproducibility of pressure value over time. Now 5-way proportional valve driven by a quasi-logic controller is installed, allowing high stability and reproducibility of stabilized pressure.
3. Up to 6 thermocouples can be connected to determine the temperature gradient over the sample up to 950°C.
4. Above 500°C, infrared temperature measurement can be used. The infrared curve shows when the temperature exceeds 500°C (Figure 4)
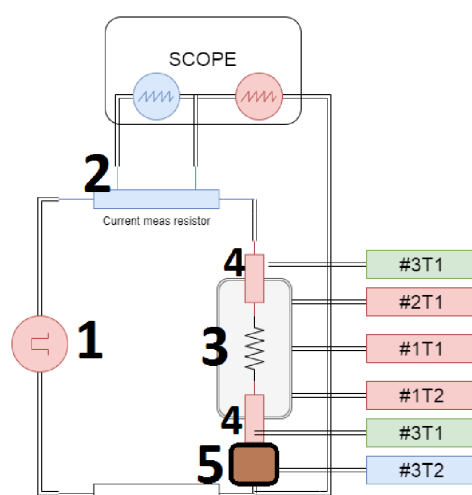
Figure 5. Schematic diagram of modernized SPS device
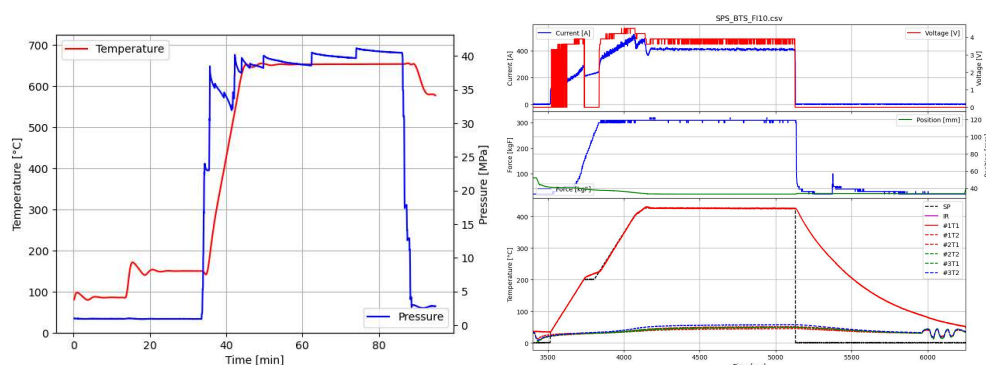
**Figure 6.** Data collected before and after apparatus development

Extending the capabilities (both process control and process parameters monitoring) enabled conducting nonstandard processes, such as SHS reaction and allows to gain detailed process information.

3. Results

### 3.1. Thermoelectric properties of arc-melted and sps-sintered materials

Figure 7 presents the electric properties of hafnium doped $Co_4Sb_{11.5}Te_{0.5}$. The samples HCST-05 and HCST-10 showed and increasement of absolute values of Seebeck coefficient. The addition of lower amounts of Hafnium has no visible impact on Seebeck coefficient. The addition of hafnium has low, but visible impact on electrical conductivity of material, lowering electrical conductivity with the hafnium amount increase.
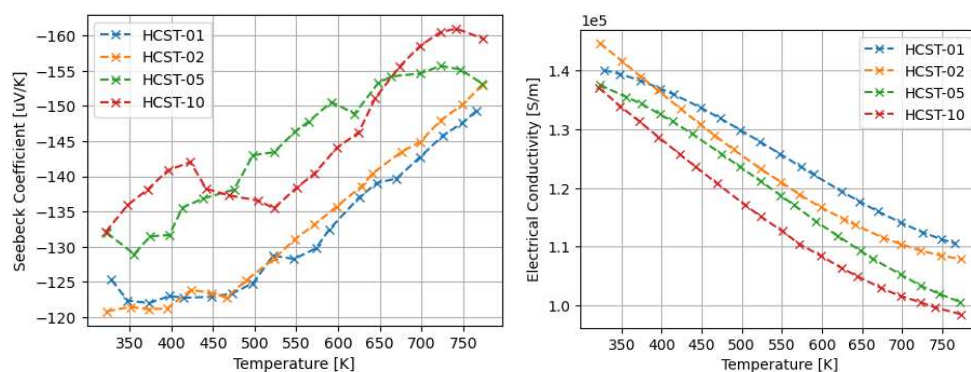
Figure 7. Transport properties of hafnium doped cobalt triantimonide (a) Seebeck coefficient and electrical conductivity (b) Heat conductivity

For the materials from the $Hf_xCo_4Sb_{11.5}Te_{0.5}$ series obtained by arc melting, the doping effect is visible for $x = 0.05$ and $x = 0.10$. With increasing Hf content, we observe a slight increase in the Seebeck coefficient and a decrease in electrical conductivity (7). However, the noticeable reduction in thermal conductivity occurs only for $x = 0.10$.
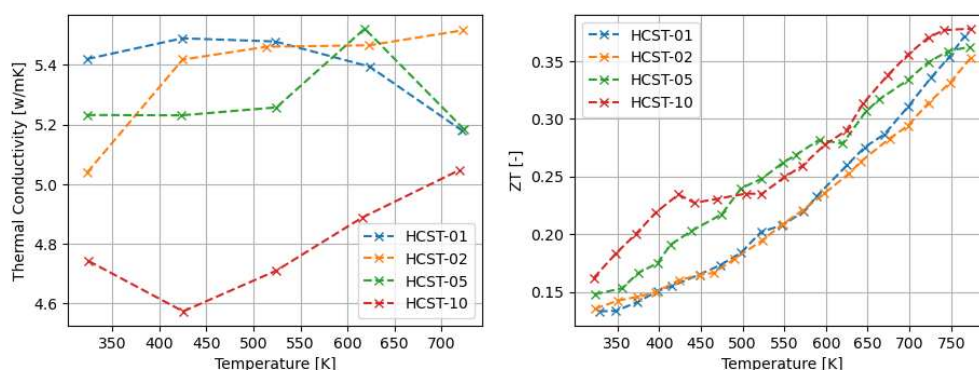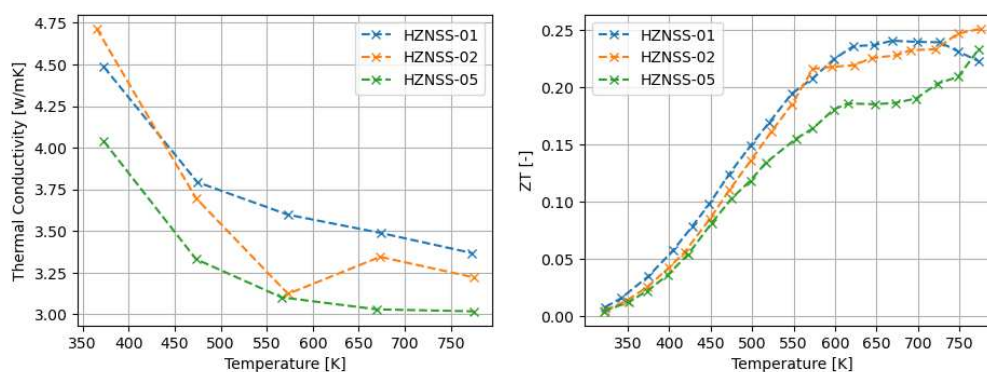

Figure 8. Figure of Merit(ZT) factor of synthesized thermoelectric materials.

Figure 9 presents electrical parameters of HZNSS half-Heusler materials. A slight Seebeck coefficient and electrical conductivity drop can be observed with the addition of Sb.
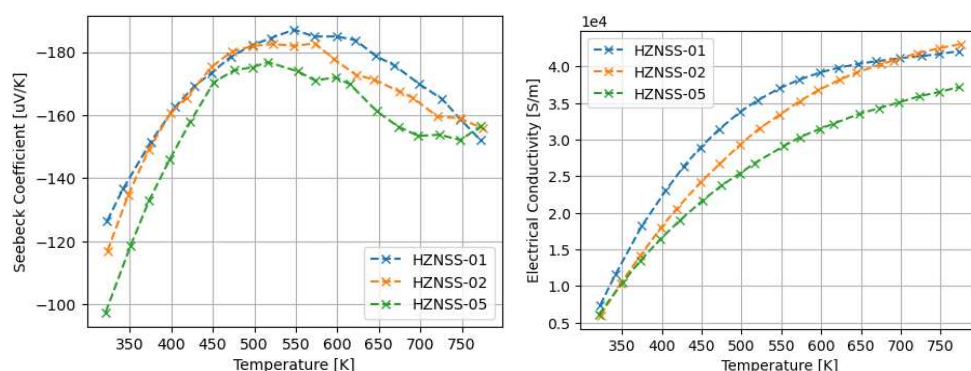
Figure 9. Transport properties of HZNSS half-Heusler material (a) Seebeck coefficient and electrical conductivity (b) Heat conductivity

Figure 10 presents thermal conductivity and ZT parameter of HZNSS samples. The thermal conductivity of HZNSS samples drops with the increase of Sb content. The ZT parameter of HZNSS materials shows similar values below 500K and lowers with the increase of Sb above 500K.

Figure 10. Figure of Merit(ZT) of synthesized thermoelectric materials.

3.2. SHS synthesis results

The following section is subdivided into two paragraphs, describing the process of SHS synthesis and presenting fabricated materials' parameters.

3.2.1. Analysis of stages of SHS synthesis

The effectiveness of the synthesis was confirmed based on the analysis of the X-ray diffraction of the material, the Figure 11 shows the diffractogram of the material at various stages of synthesis.
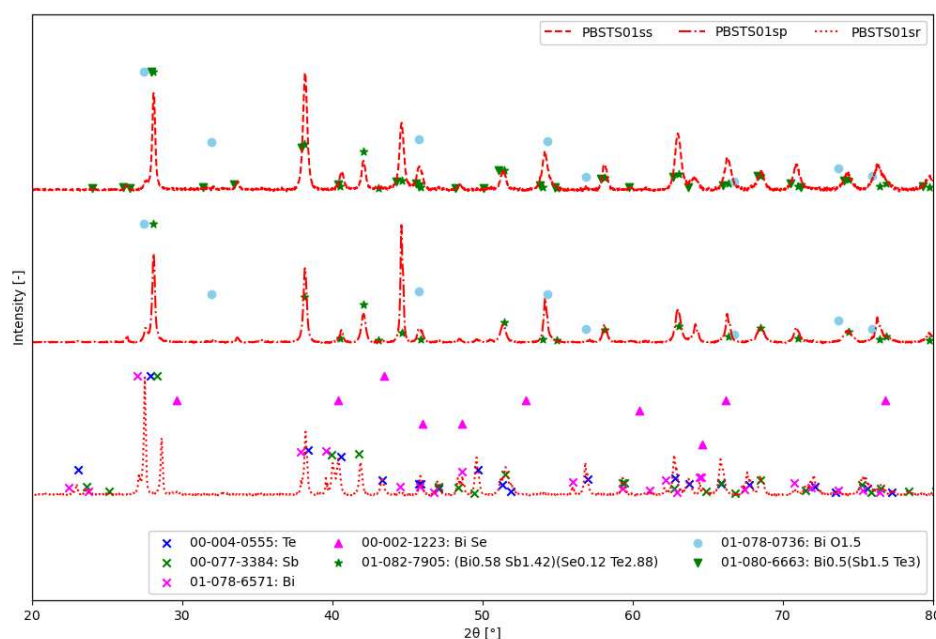
Figure 11. XRD patterns of material on different stages of synthesis; PBSTS01ss - material after SPS sintering; PBSTS01sp - material after SHS synthesis; PBSTS01sr - powder before SHS synthesis

The analysis of the diffractogram of the powder after SHS synthesis showed partial reaction of the substrates - both reflections from the substrates and the product are visible. After re-grinding and sintering, the material showed a high degree of conversion, XRD analysis did not show the presence of significant amounts of starting elements. The sample was heated at 200°C for 2 hours to test the temperature stability of the material - the last diffractogram showed no changes in the phase composition of the compound.

1. PBSTS01sr - Material after the homogenization process in an automatic mortar. The analysis of the phase composition, in addition to confirming the presence of pure elements, i.e. tellurium

(00-004-0555), antimony (00-077-3384) and bismuth (01-078-6571), also showed the presence of bismuth selenide (00-002-1223) in materials with higher selenium amount.

2. PBSTS01sp - the fragmented material after synthesis *SHS* consisted mainly of the phase $(Bi_{0.58}Sb_{1.42})(Se_{0.12}Te_{2.88})$ (01-082-7905) and bismuth oxide (01-078-0736). Some of the reflections are difficult to distinguish due to their overlap.

3. PBSTS01ss - the material after sintering using the *SPS* technique contained the $Bi_{0.5}(Sb_{1.5}Te_3)$ phase and, probably, bismuth oxide (01-078-0736)

Figure 12 presents an XRD patterns for all 4 PBSTS composition samples after SPS sintering. PBSTS01ss sample contains mostly $Bi_{0.5}Sb_{1.5}Te_3$ phase and small amounts of $(Bi_{0.58}Sb_{1.42})(Se_{0.12}Te_{2.88})$ and oxide phases. With the increase of Se content materials contain multiple phases of Bi-Sb-Te-Se phases and a oxide phase.
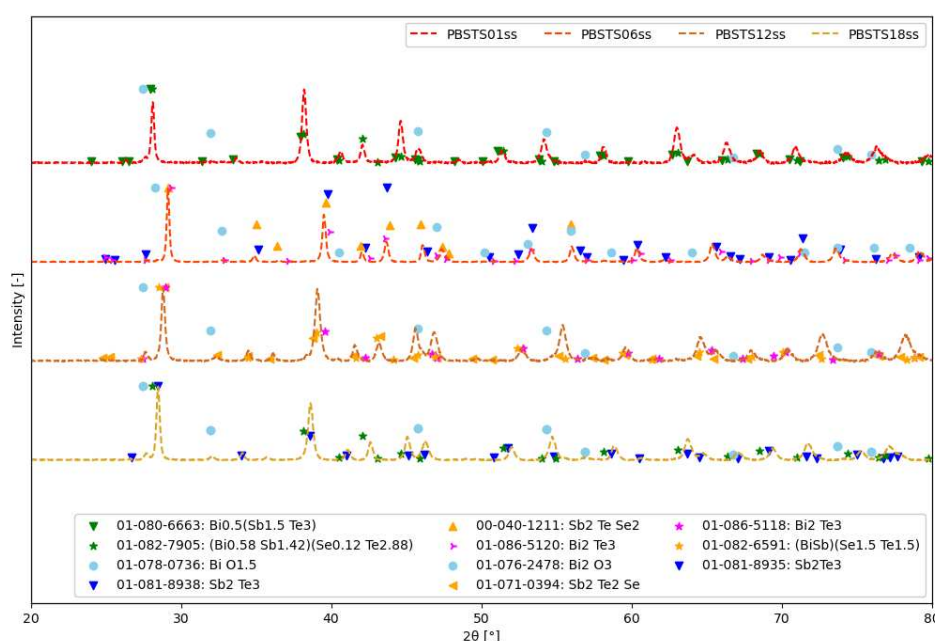

**Figure 12.** XRD patterns of samples with different selenium content

3.2.2. Thermoelectric properties of SHS synthesized bismuth telluride

The results of Seebeck coefficient measurements for the *PBSTq* material (Figure 13) showed high stability of the Seebeck coefficient as a function of temperature, in the range of 50-150°C. The introduction of a small amount of selenium into the structure causes an increase in the Seebeck coefficient by 10% (for the *PBSTS*01*s* and *PBSTS*01*q* compositions in relation to the undoped *PBSTq* material), but a further increase in the selenium content results in a significant decrease in the Seebeck coefficient.
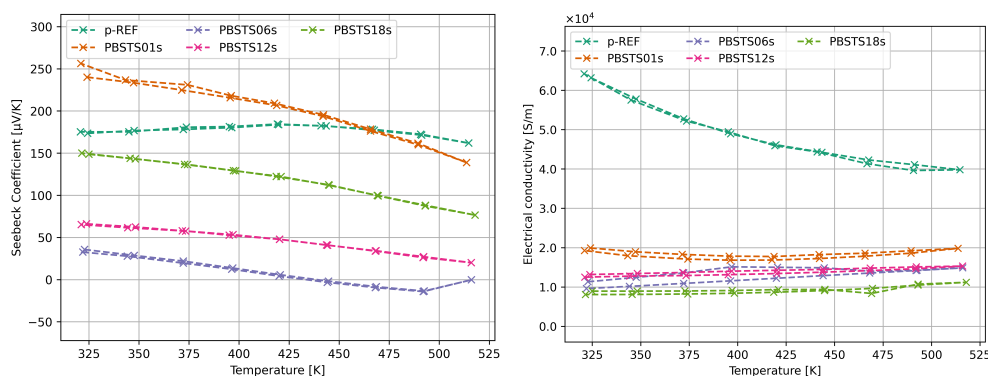
Figure 13. Seebeck coefficient and electrical conductivity of SHS-synthesized bismuth telluride samples with different selenium quotient

The PBSTS samples thermal conductivity lowers with increasing the selenium content. The *ZT* factor of PBSTS01s sample equals about half value of reference material (Figure 14).
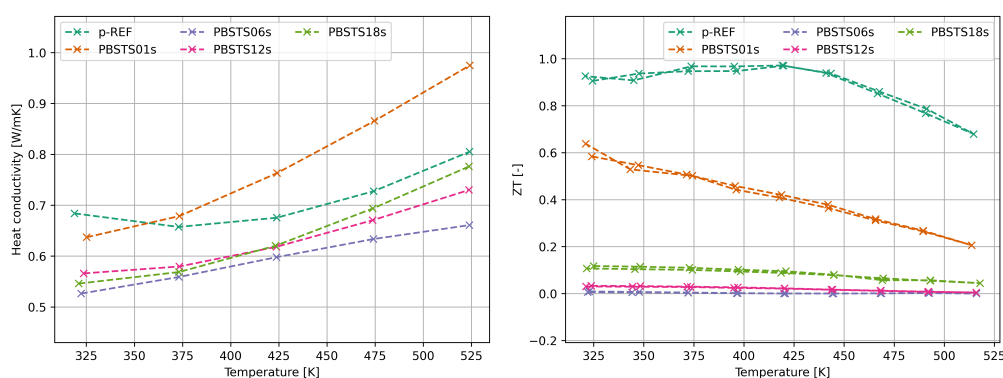
Figure 14. Seebeck coefficient of SHS-synthesized bismuth telluride samples with different selenium quotient

4. Discussion

The modernized SPS device allowed for gaining information about process dynamics, which was a key information while optimization of SHS synthesis parameters. Most devices and descriptions analyzes SPS process basing on the 3 main parameters: maximum temperature, time and applied pressure [2,28]. The extension of collected parameters allowed for continues monitoring of process parameters, which can be needed for understanding the phenomenons and stages of sintering process.

4.1. The properties of Arc-Melted materials

The thermal conductivity of cobalt triantimonide material HCST was lowered in the case of HCST-10 sample - this suggests that the hafnium influences mostly micro-structure of the material, with a smaller affect on electron structure. The HZNSS materials exhibited similar thermoelectric properties, although Seebeck coefficient and electrical conductivity, thermal conductivity droped with increase of Sb content in the sample.

Due to low concentration of hafnium (HCST) and antimony(HZNSS) it was nearly impossible to examine phase difference within fabricated materials using XRD or SEM methods, but due to Seebeck coefficient sensitivity on chemical and phase composition it was possible to distinguish differences between HCST-[01,02] and HCST-[05-10] materials.

4.2. SHS synthesis

Conducted SHS synthesis yielded the fabrication p-type bismuth-telluride material. Despite oxide phases were identified in all materials fabricated by SHS method, the analysis of ZT factor (Figure 14) shows, that there is possible to fabricate material characterized with $ZT \simeq 0.5$ with a significant reduction of processing time and energy consumed during synthesis.

4.3. Thermoelectric properties of SHS materials

Compared to the results presented in the work [29], the values of the Seebeck coefficients obtained in the presented work for *p*-type materials are less dependent on temperature [29]. A noteworthy achievement is the $PBSTq$ material, characterized with almost constant, stable over time and temperature α coefficient for the. The *p* material obtained as part of the work, undoped with selenium (pREF), had a Seebeck coefficient ranging from $165\frac{\mu V}{K}$ to $185\frac{\mu V}{K}$, which is approximately $20\frac{\mu V}{K}$ higher than those presented in the work [30]. The nature of the Seebeck coefficient dependence is also similar for the $Bi - Sb - Te - Se$ compound with a small amount of selenium, although in this case an increase in the coefficient value of approximately $40\frac{\mu V}{K}$ was observed (Figure 15). In the work [31] the material $Bi_{0.5}Sb_{1.5}Te_{3-x}Se_x$ was tested in the range $0 \leftrightarrow 0.1$. Modification of the material with selenium in the tested range resulted in the standardization of the Seebeck coefficient in the target operating temperature range (The characteristics of the Seebeck coefficient are shown in Figure 15a). The authors indicate the possibility of increasing the Seebeck coefficient by introducing a 3% surplus of tellurium. The Seebeck coefficient characteristics of the tellurium surplus material are shown in Figure 15b.
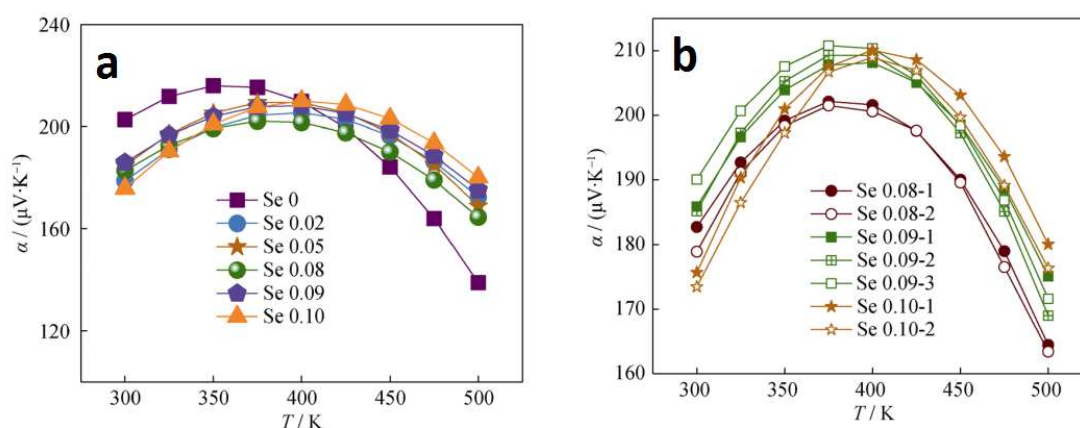
Figure 15. Dependence of the Seebeck coefficient a) for the material $Bi_{0.5}Sb_{1.5}Te3 - xSe_x$; b) for material with 3% tellurium surplus [31].

The amount of selenium in the range $0.01 < x < 0.1$ does not affect the thermal properties of the material, increasing the Seebeck coefficient by 10%. Further increasing the amount of selenium results in a decrease in the Seebeck coefficient of the material, which is caused by the formation of *n* zones in the material.

5. Conclusions

This publication shows the possibility of extension and adaptation SPS system for synthesis and fabrication of semiconductor materials. The multi-point measurement allowed precise control of process parameters which obtains many additional information about process.

Abbreviations

The following abbreviations are used in this manuscript:

SPS   Spark Plasma Sintering
SHS   Self-propagating high-temperature synthesis
AM   Arc-Melting
ZT   Thermoelectric Figure-of-merit

References

1. Ratzker, B.; Sokol, M. Exploring the capabilities of high-pressure spark plasma sintering (HPSPS): A review of materials processing and properties. *Materials and Design* **2023**, *233*, 112238. doi:https://doi.org/10.1016/j.matdes.2023.112238.

2. Cincotti, A.; Locci, A.; Orrù, R.; Cao, G. Modeling of SPS apparatus: Temperature, current and strain distribution with no powders. *AIChE journal* **2007**, *53*, 703–719.

3. Stuer, M.; Bowen, P.; Zhao, Z. Spark Plasma Sintering of Ceramics: From Modeling to Practice. *Ceramics* **2020**, *3*, 476–493. doi:10.3390/ceramics3040039.

4. Nosewicz, S.; Jurczak, G.; Chrominski, W.; Rojek, J.; Kaszyca, K.; Chmielewski, M. Combined EBSD and Computer-Assisted Quantitative Analysis of the Impact of Spark Plasma Sintering Parameters on the Structure of Porous Materials. *Metallurgical and Materials Transactions A* **2022**, *53*, 4101?4125. doi:10.1007/s11661-022-06821-z.

5. Saleemi, M.; Toprak, M.S.; Li, S.; Johnsson, M.; Muhammed, M. Synthesis, processing, and thermoelectric properties of bulk nanostructured bismuth telluride (Bi2Te3). *J. Mater. Chem.* **2012**, *22*, 725?730. doi:10.1039/c1jm13880d.

6. Lim, S.S.; Jung, S.J.; Kim, B.K.; Kim, D.I.; Lee, B.H.; Won, S.O.; Shin, J.; Park, H.H.; Kim, S.K.; Kim, J.S.; Baek, S.H. Combined hot extrusion and spark plasma sintering method for producing highly textured thermoelectric Bi2Te3 alloys. *Journal of the European Ceramic Society* **2020**, *40*, 3042–3048. doi:https://doi.org/10.1016/j.jeurceramsoc.2020.03.008.

7. Kim, H.S.; Liu, W.; Chen, G.; Chu, C.W.; Ren, Z. Relationship between thermoelectric figure of merit and energy conversion efficiency. *Proceedings of the National Academy of Sciences* **2015**, *112*, 8205–8210, [https://www.pnas.org/doi/pdf/10.1073/pnas.1510231112]. doi:10.1073/pnas.1510231112.

8. Park, O.; Park, S.J.; Kim, H.S.; Lee, S.W.; Heo, M.; il Kim, S. Enhanced thermoelectric transport properties of Bi2Te3 polycrystalline alloys via carrier type change arising from slight Pb doping. *Materials Science in Semiconductor Processing* **2023**, *166*, 107723. doi:https://doi.org/10.1016/j.mssp.2023.107723.

9. Hu, X.; Fan, X.; Feng, B.; Kong, D.; Liu, P.; Xu, C.; Kuang, Z.; Li, G.; Li, Y. Decoupling Seebeck coefficient and resistivity, and simultaneously optimizing thermoelectric and mechanical performances for n-type BiTeSe alloy by multi-pass equal channel angular extrusion. *Materials Science and Engineering: B* **2021**, *263*, 114846. doi:https://doi.org/10.1016/j.mseb.2020.114846.

10. Dongre, B.; Carrete, J.; Wen, S.; Ma, J.; Li, W.; Mingo, N.; Madsen, G.K.H. Combined treatment of phonon scattering by electrons and point defects explains the thermal conductivity reduction in highly-doped Si. *Journal of Materials Chemistry A* **2020**, *8*, 1273?1278. doi:10.1039/c9ta11424f.

11. Mao, J.; Niedziela, J.L.; Wang, Y.; Xia, Y.; Ge, B.; Liu, Z.; Zhou, J.; Ren, Z.; Liu, W.; Chan, M.K.; Chen, G.; Delaire, O.; Zhang, Q.; Ren, Z. Self-compensation induced vacancies for significant phonon scattering in InSb. *Nano Energy* **2018**, *48*, 189–196. doi:https://doi.org/10.1016/j.nanoen.2018.03.058.

12. d?Angelo, M.; Galassi, C.; Lecis, N. Thermoelectric Materials and Applications: A Review. *Energies* **2023**, *16*. doi:10.3390/en16176409.

13. Marchenkov, V.V.; Lukoyanov, A.V.; Baidak, S.T.; Perevalova, A.N.; Fominykh, B.M.; Naumov, S.V.; Marchenkova, E.B. Electronic Structure and Transport Properties of Bi2Te3 and Bi2Se3 Single Crystals. *Micromachines* **2023**, *14*. doi:10.3390/mi14101888.

14. Yang, J.; Aizawa, T.; Yamamoto, A.; Ohta, T. Thermoelectric properties of n-type (Bi2Se3)x(Bi2Te3)1?x prepared by bulk mechanical alloying and hot pressing. *Journal of Alloys and Compounds* **2000**, *312*, 326–330. doi:https://doi.org/10.1016/S0925-8388(00)01159-2.

15. Bucholc, B.; Kaszyca, K.; ?piewak, P.; Mars, K.; Kruszewski, M.J.; Ciupi?ski, u.; Kowiorski, K.; Zyba?a, R. Thermoelectric properties of bismuth-doped magnesium silicide obtained by the self-propagating high-temperature synthesis. *Bulletin of the Polish Academy of Sciences Technical Sciences* **2022**, *70*, e141007. doi:10.24425/bpasts.2022.141007.

16. Liu, R.; Tan, X.; Ren, G.; Liu, Y.; Zhou, Z.; Liu, C.; Lin, Y.; Nan, C. Enhanced Thermoelectric Performance of Te-Doped Bi2Se3?xTex Bulks by Self-Propagating High-Temperature Synthesis. *Crystals* **2017**, *7*. doi:10.3390/cryst7090257.

17. Zheng, G.; Su, X.; Liang, T.; Lu, Q.; Yan, Y.; Uher, C.; Tang, X. High thermoelectric performance of mechanically robust n-type Bi2Te3?xSex prepared by combustion synthesis. *Journal of Materials Chemistry A* **2015**, *3*, 6603?6613. doi:10.1039/c5ta00470e.

18. R. Knight, R.W.S.; Apelian, D. Application of plasma arc melting technology to processing of reactive metals. *International Materials Reviews* **1991**, *36*, 221–252, [https://doi.org/10.1179/imr.1991.36.1.221]. doi:10.1179/imr.1991.36.1.221.

19. Aversano, F.; Palumbo, M.; Ferrario, A.; Boldrini, S.; Fanciulli, C.; Baricco, M.; Castellero, A. Role of secondary phases and thermal cycling on thermoelectric properties of TiNiSn half-Heusler alloy prepared by different processing routes. *Intermetallics* **2020**, *127*, 106988. doi:https://doi.org/10.1016/j.intermet.2020.106988.

20. Zhang, J.; Hu, Y.; Wei, Q.; Xiao, Y.; Chen, P.; Luo, G.; Shen, Q. Microstructure and mechanical properties of RexNbMoTaW high-entropy alloys prepared by arc melting using metal powders. *Journal of Alloys and Compounds* **2020**, *827*, 154301. doi:https://doi.org/10.1016/j.jallcom.2020.154301.

21. Cieslak, J.; Tobola, J.; Berent, K.; Marciszko, M. Phase composition of AlxFeNiCrCo high entropy alloys prepared by sintering and arc-melting methods. *Journal of Alloys and Compounds* **2018**, *740*, 264–272. doi:https://doi.org/10.1016/j.jallcom.2017.12.333.

22. Zhang, J.; Xiong, K.; Huang, L.; Xie, B.; Ren, D.; Tang, C.; Feng, W. Effect of Doping with Different Nb Contents on the Properties of CoCrFeNi High-Entropy Alloys. *Materials* **2023**, *16*. doi:10.3390/ma16196407.

23. Yamada, O.; Miyamoto, Y.; Koizumi, M. Self-Propagating High-Temperature Synthesis (SHS) of SiC Powders and the Properties of the Sintered Compact. *Journal of the Japan Society of Powder and Powder Metallurgy* **1986**, *33*, 286–290. doi:10.2497/jjspm.33.286.

24. Moskovskikh, D.O.; Mukasyan, A.S.; Rogachev, A.S. Self-propagating high-temperature synthesis of silicon carbide nanopowders. *Doklady Physical Chemistry* **2013**, *449*, 41–43. doi:10.1134/S0012501613030032.

25. Yasenchuk, Y.; Marchenko, E.; Gunther, V.; Radkevich, A.; Kokorev, O.; Gunther, S.; Baigonakova, G.; Hodorenko, V.; Chekalkin, T.; Kang, J.h.; Weiss, S.; Obrosov, A. Biocompatibility and Clinical Application of Porous TiNi Alloys Made by Self-Propagating High-Temperature Synthesis (SHS). *Materials* **2019**, *12*. doi:10.3390/ma12152405.

26. Kruszewski, M.; Kot, M.; Cymerman, K.; Chmielewski, M.; Moszczy?ska, D.; Ma?ek, M.; Ciupi?ski, . Rapid fabrication of Se-modified skutterudites obtained via self-propagating high-temperature synthesis and pulse plasma sintering route. *Ceramics International* **2023**, *49*, 9560–9565. doi:https://doi.org/10.1016/j.ceramint.2022.11.124.

27. Min, S.; Blumm, J.; Lindemann, A. A new laser flash system for measurement of the thermophysical properties. *Thermochimica Acta* **2007**, *455*, 46–49. 6th KSTP Symposium, doi:https://doi.org/10.1016/j.tca.2006.11.026.

28. Ratzker, B.; Sokol, M.; Kalabukhov, S.; Frage, N. Creep of Polycrystalline Magnesium Aluminate Spinel Studied by an SPS Apparatus. *Materials* **2016**, *9*. doi:10.3390/ma9060493.

29. Qiu, J.; Yan, Y.; Xie, H.; Luo, T.; Xia, F.; Yao, L.; Zhang, M.; Zhu, T.; Tan, G.; Su, X.; Wu, J.; Uher, C.; Jiang, H.; Tang, X. Achieving superior performance in thermoelectric Bi0.4Sb1.6Te3.72 by enhancing texture and inducing high-density line defects. *Science China Materials* **2021**, *64*, 1507–1520. doi:10.1007/s40843-020-1548-x.

30. Guo, X.; Jia, X.; Jie, K.; Sun, H.; Zhang, Y.; Sun, B.; Ma, H. Thermoelectric transport properties and crystal growth of BiSbTe3 bulk materials produced by a unique high-pressure synthesis. *CrystEngComm* **2013**, *15*, 7236–7242. doi:10.1039/C3CE40780B.

31. Zhai, R.S.; Wu, Y.H.; Zhu, T.J.; Zhao, X.B. Thermoelectric performance of p-type zone-melted Se-doped Bi0.5Sb1.5Te3 alloys. *Rare Metals* **2018**, *37*, 308–315. doi:10.1007/s12598-018-1005-2.